

Design of Frequency-Dependent Weighting Functions for H_2 Control of Seismic-Excited Structures

KYUNG-WON MIN

LAN CHUNG

Department of Architectural Engineering, Dankook University, Seoul, Korea

SEOK-JUN JOO

T.E. Solution Co. Ltd, Seoul, Korea

JINKOO KIM

Department of Architectural Engineering, Sungkyunkwan University, Suwon, Korea
jinkoo@yurim.skku.ac.kr

(Received 19 December 2002; accepted 12 July 2004)

Abstract: In this paper we investigate a systematic procedure for determining frequency-dependent weighting functions for an H_2 controller in the frequency domain. Based on experimental results from the system identification of a model structure with an active mass driver, we choose frequency-dependent weighting functions, including filters on an earthquake input model, sensor noise, control output, and control force. These are incorporated into the plant to produce an optimal controller. Combining the weighting functions and filters and comparing the trade-off problem between response reduction and control force, an optimal combination of weighting functions and filters is determined. The performance of the designed H_2 controller is evaluated by shaking-table tests of a three-story scaled model with an active mass driver.

Key Words: Structural control, H_2 controller, weighting functions, active mass driver

1. INTRODUCTION

Linear quadratic Gaussian control (LQG), which is a linear quadratic regulator (LQR) combined with a Kalman filter, has been widely used in the active control of building structures. It is designed in the time domain, and has proven to be effective in reducing the dynamic response of structures. However, it requires an iterative procedure to obtain the weighting matrix to be used as a performance index, because there is no definite criterion for selecting a weighting matrix.

Recently, frequency domain control laws have been applied in civil structures, which provide the control designer with frequency representations of both the structure and the excitation during control design (Spencer et al., 1994). These allow the designer to specify disturbance attenuation over a desired frequency range, as well as to roll off the control action at high frequencies where measurement noise and uncertainties may plague the controlled

structure. The transfer function of a structure in the frequency domain can be obtained directly from modal tests, and random signals such as earthquake and wind loads can be modeled by a spectral density function in the frequency domain. Optimal control in the frequency domain can be carried out using such information obtained in the frequency domain. The performance of the controller can be further enhanced by incorporating weighting functions, which decrease the effect of the excitation in specific frequency regions and reduce difficulties associated with high-frequency control forces containing noise and uncertainties.

In the frequency domain, the desired controller can be achieved by a proper selection of frequency-dependent weighting functions and filters modeling earthquake disturbances. The H_2 control design method, one of the frequency domain control methods, gives an optimal controller by minimizing the H_2 norm of the transfer function from the input excitation (including measurement noise) to the structural responses which we desire to control (Doyle et al., 1989). Dyke et al. (1994) developed a mathematical model for a scaled building structure through system identification in the frequency domain. They designed an H_2 controller using dynamic feedback of acceleration responses and verified its performance by experiments. Suhardjo et al. (1992) and Spencer et al. (1994) have proposed optimal design procedures in the frequency domain. They have shown that frequency domain control laws are flexible and offer a good match between control concepts and engineering practice. Previous research focused on the application of the frequency domain design method to building structures and experimental verifications. However, they did not address one of the main advantages of the frequency domain design, which is to shape the structural response output in a desirable manner by the proper selection and combination of variously defined weighting functions.

In this paper we propose a systematic procedure for determining frequency-dependent weighting functions in designing an H_2 controller. The prototype frequency-dependent weighting functions, such as for an earthquake input model, sensor measurement noise, control force to prevent spillover, and control output, are formulated first, and the prototype functions are combined to design an optimal controller. The selected weighting functions are applied in shaking-table tests of a scaled three-story shear-building model with an active mass driver (AMD) to validate their performances.

2. H_2 CONTROLLER

A transfer function represents the relation between the input vector, $\mathbf{u}(t)$, and the output vector, $\mathbf{y}(t)$. For a linear system, the input and output are related in the Laplace domain as follows

$$\mathbf{Y}(s) = \mathbf{H}(s)\mathbf{U}(s) \quad (1)$$

where $\mathbf{Y}(s)$ and $\mathbf{U}(s)$ are the Laplace transforms of $\mathbf{y}(t)$ and $\mathbf{u}(t)$, respectively, and $\mathbf{H}(s)$ is the transfer function matrix from $\mathbf{u}(t)$ to $\mathbf{y}(t)$. If $\mathbf{u}(t)$ is a random process and $\mathbf{S}_u(\omega)$ is the power spectral density function (PSDF) of $\mathbf{u}(t)$, then the corresponding PSDF of the output vector $\mathbf{y}(t)$ can be represented as follows

$$\mathbf{S}_y(\omega) = \mathbf{H}(j\omega)\mathbf{S}_u(\omega)\mathbf{H}^*(j\omega) \quad (2)$$

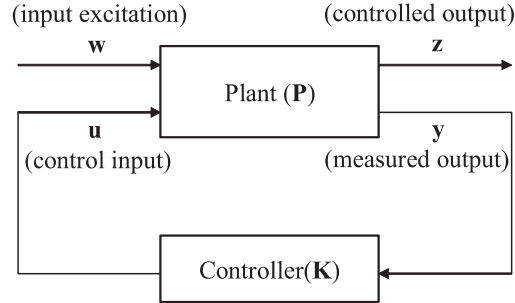


Figure 1. Basic block diagram for a control problem.

where \mathbf{T}^* denotes the conjugate transpose matrix of \mathbf{T} , and j is an imaginary constant. The root mean square (RMS) value of output $\mathbf{y}(t)$ is obtained as follows:

$$\|\mathbf{y}\|_{RMS} = \sqrt{\text{trace} \left\{ \frac{1}{2\pi} \int \int \int_{-\infty}^{\infty} \mathbf{H}(j\omega) \mathbf{S}_u(\omega) \mathbf{H}^*(j\omega) d\omega \right\}}. \quad (3)$$

When the input $\mathbf{u}(t)$ is a unit white noise (i.e. $\mathbf{S}_u(\omega) = \mathbf{I}$, where \mathbf{I} is the unit matrix), the 2-norm of the transfer function \mathbf{H} is defined as follows (Boyd and Barratt, 1991):

$$\|\mathbf{H}\|_2 = \sqrt{\text{trace} \left\{ \frac{1}{2\pi} \int \int \int_{-\infty}^{\infty} \mathbf{H}(j\omega) \mathbf{H}^*(j\omega) d\omega \right\}}. \quad (4)$$

Therefore, the 2-norm of the transfer function represents the RMS value of the output when the input is a unit white-noise vector.

Figure 1 shows the general block diagram representing the control problem, where \mathbf{y} is the measured structural response vector, \mathbf{z} is the response vector to be controlled, \mathbf{u} is the control input vector, and \mathbf{w} is the input excitation vector. The control output \mathbf{z} is composed of the linear combination of the state of the system and the control force \mathbf{u} , and it can have various forms according to the control objective. The goal of the H_2 control is to design a controller \mathbf{K} which minimizes the 2-norm of the transfer function from the excitation input \mathbf{w} to the control output $\mathbf{H}_{z\mathbf{w}}$, while maintaining the system stability.

3. CONTROL FORMULATION

3.1. Plant Model

Experimental investigations have been performed to evaluate the performance of the designed H_2 controller. The test structure, which is shown in Figure 2, is a three-story, single-bay steel frame with story height of 40 cm, plan dimension of $60 \times 60 \text{ cm}^2$, and story mass of 16 kg. The structure is excited on a uniaxial shaking table by an AC servomotor and is



Figure 2. Photograph of the experimental setup.

controlled by a separate computer through a National Instrument (NI) LAB-PC-1200 D/A board and an NI BNC-2081 board. The control force is supplied by an AMD attached to the top floor of the test structure. The AMD shown in Figure 3 is composed of a moving mass of 4.7 kg, a ball screw unit, and an AC servomotor. The maximum stroke of the AMD is ± 150 mm with the maximum acceleration capacity of 500 cm s^{-2} .

The accelerometers are positioned on each floor of the structure to measure the absolute accelerations of the test structure. Additionally, accelerometers located on the AMD and on the base measure the absolute accelerations of the AMD and the ground excitation. The data acquisition and implementation of the digital controller are performed using a real-time digital signal processor (DSP). The primary tasks of the data acquisition board are to perform the analog-to-digital (A/D) conversion of the measured acceleration data and to perform the digital-to-analog (D/A) conversion of the command signal computed by the control program. A 16-channel data acquisition system is employed using an NI PCI-MIO-16XE-50 board and an NI BNC-2090 board. A schematic diagram of the test system is presented in Figure 4. The natural frequencies are found experimentally to be 2.8, 7.9, and 12.2 Hz by investigating the responses of white-noise excitation. Also, the fundamental modal damping ratio is found to be 1.1%.

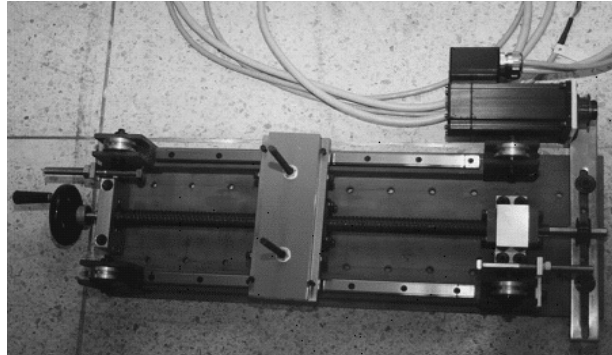


Figure 3. Active mass driver.

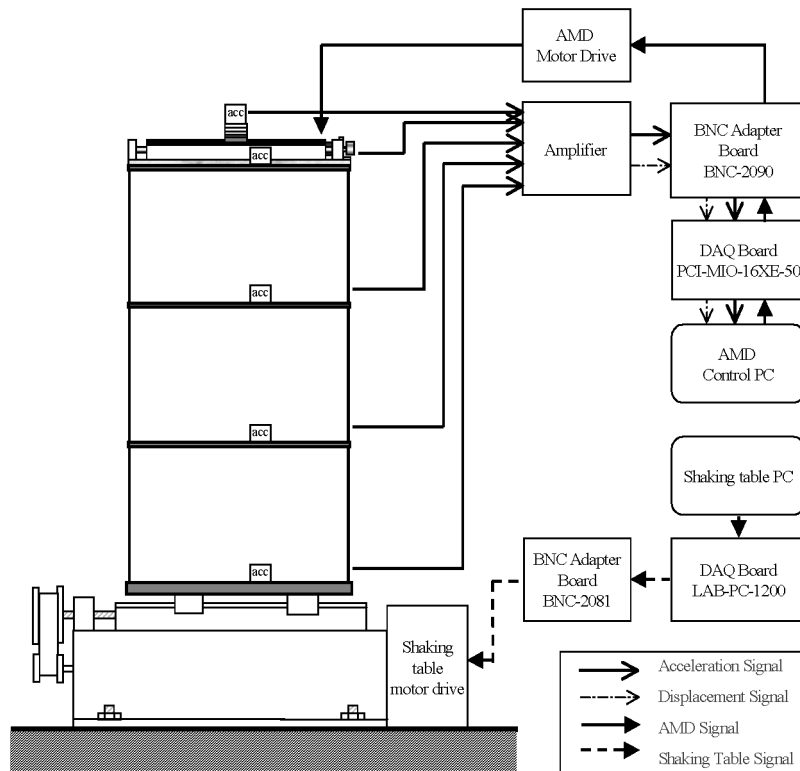


Figure 4. Schematic diagram of the test system.

The plant includes the building structure, the AMD, filters, and weighting functions in the frequency domain. Figure 5 illustrates the block diagram for the seismic response control system, where w_g and w_s represent the ground acceleration input and the sensor noise included in the measured signal, respectively, both of which are modeled as white-noise

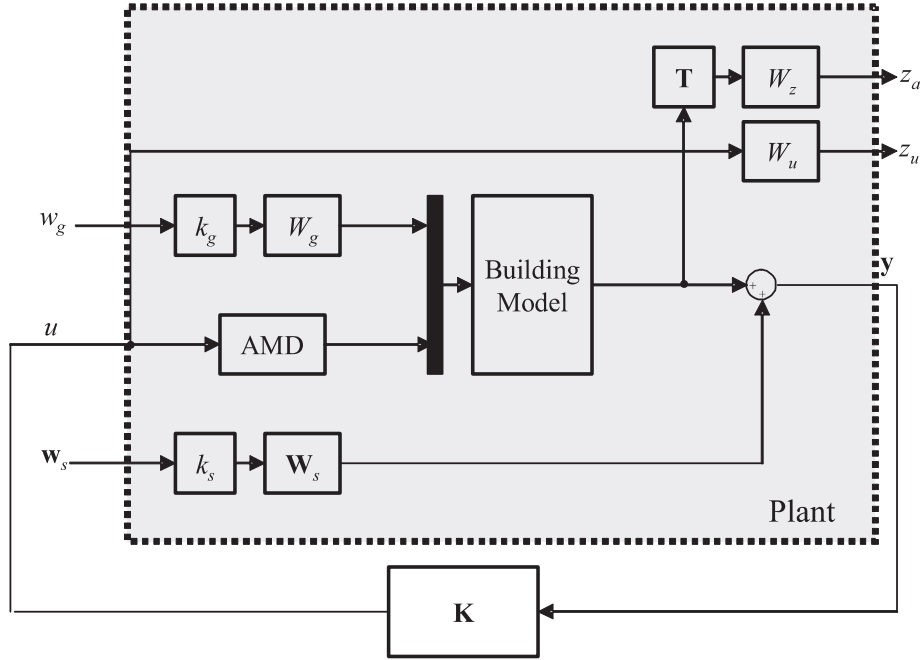


Figure 5. Block diagram for a seismic response control system.

disturbances. A filter W_g is used for the shaping of the frequency contents of the input excitation. W_s is the frequency-dependent weighting function for the sensor noise. z_a is the absolute acceleration at the top floor multiplied by the weight function W_z , and z_u is the control input multiplied by the weight function W_u . The reason for designating the acceleration at the top floor as the controlled output z_a is to enhance the serviceability of the building by minimizing the top floor acceleration, which is usually the maximum acceleration of all floors. The weighting functions W_z and W_u are chosen considering the trade-off between the control outputs z_a and z_u . \mathbf{y} represents the measured absolute acceleration in each floor, which is fed back to determine the control force, and u is the input signal for the AMD motor, which corresponds to the output of the controller \mathbf{K} . \mathbf{T} is the constant matrix dictating the component of the structural response comprising the regulated response vector z_a .

The input and output of the plant, which are the input excitation \mathbf{w} and the control output \mathbf{z} , respectively, are represented as follows:

$$\mathbf{w} = [w_g \quad \mathbf{w}_s]^T \tag{5}$$

$$\mathbf{z} = [z_a \quad z_u]^T. \tag{6}$$

The set of controllers, denoted \mathbf{K} , internally stabilizes the closed-loop feedback system shown in Figure 1 or in Figure 5, and makes their transfer function matrices proper. Among those controllers stabilizing the system, the H_2 controller is obtained by minimizing the H_2 norm of the transfer function $\mathbf{H}_{z\mathbf{w}}$ as follows:

$$\min_{\mathbf{K} \in \mathbf{K}_s} \|\mathbf{H}_{zw}\|_2. \quad (7)$$

To obtain the transfer function \mathbf{H}_{zw} , the system transfer function matrix \mathbf{P} , as shown in Figure 1, is partitioned as follows:

$$\mathbf{P} = \begin{bmatrix} \mathbf{P}_{zw} & \mathbf{P}_{zu} \\ \mathbf{P}_{yw} & \mathbf{P}_{yu} \end{bmatrix}. \quad (8)$$

Then the transfer function from \mathbf{w} to \mathbf{z} can be written as (Calise and Sweriduk, 1998)]

$$\mathbf{H}_{zw} = \mathbf{P}_{zw} + \mathbf{P}_{zu} \mathbf{K} (\mathbf{I} - \mathbf{P}_{yu} \mathbf{K})^{-1} \mathbf{P}_{yw} \quad (9)$$

where \mathbf{P} is assumed to be proper, and \mathbf{K} is the controller which stabilizes the system. Referring to the block diagram representation shown in Figure 5, the partitioned elements of the system transfer function matrix \mathbf{P} are given by

$$\mathbf{P}_{zw} = \begin{bmatrix} P_{z_a w_g} & P_{z_a w_s} \\ P_{z_u w_g} & P_{z_u w_s} \end{bmatrix} = \begin{bmatrix} k_g W_z \mathbf{T} \mathbf{G}_1 W_g & \mathbf{0} \\ 0 & \mathbf{0} \end{bmatrix} \quad (10)$$

$$\mathbf{P}_{zu} = \begin{bmatrix} P_{z_a u} \\ P_{z_u u} \end{bmatrix} = \begin{bmatrix} W_z \mathbf{T} \mathbf{G}_2 G_3 \\ W_u \end{bmatrix} \quad (11)$$

$$\mathbf{P}_{yw} = \begin{bmatrix} P_{y w_g} & P_{y w_s} \end{bmatrix} = [k_g \mathbf{G}_1 W_g \quad k_s W_s] \quad (12)$$

$$\mathbf{P}_{yu} = \mathbf{G}_2 G_3, \quad (13)$$

where \mathbf{G}_1 and \mathbf{G}_2 are the transfer functions from the base acceleration of the building model to the measured acceleration \mathbf{y} , and from the relative acceleration of the AMD mass with respect to the third floor to the measured acceleration \mathbf{y} , respectively. Also, G_3 is the transfer function from the input signal of the AMD motor to the relative acceleration of the AMD.

For the identification of the combined system (i.e. the building model with the AMD), each component is identified separately by experiment and then the results are combined. The state equations for the structure and the AMD are given as

$$\text{model structure } \dot{\mathbf{x}}_s = \mathbf{A}_s \mathbf{x}_s + \mathbf{B}_{s1} \ddot{x}_g + \mathbf{B}_{s2} \ddot{x}_d \quad (14)$$

$$\mathbf{y} = \mathbf{C}_s \mathbf{x}_s + \mathbf{D}_{s2} \ddot{x}_d \quad (15)$$

$$\text{AMD } \dot{\mathbf{x}}_a = \mathbf{A}_a \mathbf{x}_a + \mathbf{B}_a u \quad (16)$$

$$\ddot{x}_d = \mathbf{C}_a \mathbf{x}_a + D_a u. \quad (17)$$

Here, \mathbf{x}_s and \mathbf{x}_a are the state vectors of the model structure and the AMD, respectively, \mathbf{y} is the vector of measured responses, \ddot{x}_d is the relative acceleration of the AMD to that of the third floor, and u is the command signal to the AMD motor. In equation (15) the ground ac-

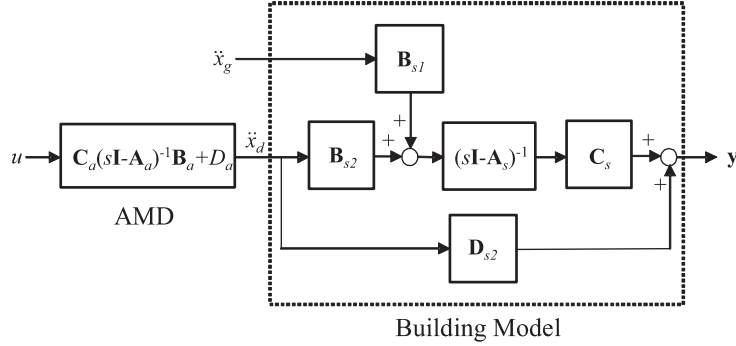


Figure 6. Block diagram for building model and AMD.

celeration input term is ignored, because numerical analysis shows that the influence matrix corresponding to the ground acceleration affects little the structural response. In addition, the ground acceleration input term is not included in the measurement equation when the absolute accelerations of the building floors are measured. The block diagram of a structure with an AMD is shown in Figure 6. The plant is composed of weighting functions used to increase control efficiency in addition to those shown in the figure.

Referring to Figure 6, \mathbf{G}_1 , \mathbf{G}_2 , and \mathbf{G}_3 , which are the partitioned elements of the system transfer function matrix, are given by

$$\mathbf{G}_1 = \mathbf{C}_s (s\mathbf{I} - \mathbf{A}_s)^{-1} \mathbf{B}_{s1} \quad (18)$$

$$\mathbf{G}_2 = \mathbf{C}_s (s\mathbf{I} - \mathbf{A}_s)^{-1} \mathbf{B}_{s2} + \mathbf{D}_{s2} \quad (19)$$

$$\mathbf{G}_3 = \mathbf{C}_a (s\mathbf{I} - \mathbf{A}_a)^{-1} \mathbf{B}_a + D_a. \quad (20)$$

By substituting equations (10)–(13) into equation (8) the transfer function \mathbf{H}_{z_w} can be obtained as follows:

$$\begin{aligned} \mathbf{H}_{z_w} &= \begin{bmatrix} \mathbf{H}_{z_a W_g} & \mathbf{H}_{z_a W_s} \\ \mathbf{H}_{z_u W_g} & \mathbf{H}_{z_u W_s} \end{bmatrix} \\ &= \begin{bmatrix} k_g W_z \mathbf{T} (\mathbf{I} - \mathbf{G}_2 \mathbf{G}_3 \mathbf{K})^{-1} \mathbf{G}_1 W_g & k_s W_z \mathbf{T} \mathbf{G}_2 \mathbf{G}_3 \mathbf{K} (\mathbf{I} - \mathbf{G}_2 \mathbf{G}_3 \mathbf{K})^{-1} W_s \\ k_g W_u \mathbf{K} (\mathbf{I} - \mathbf{G}_2 \mathbf{G}_3 \mathbf{K})^{-1} \mathbf{G}_1 W_g & k_s W_u \mathbf{K} (\mathbf{I} - \mathbf{G}_2 \mathbf{G}_3 \mathbf{K})^{-1} W_s \end{bmatrix}. \quad (21) \end{aligned}$$

Equation (21) shows that the weighted response z_a can be further decreased by increasing the weighting function W_z . Also, by increasing the weighting function W_u the weighted control input z_u can be decreased, which results in a reduction of the control force. However, there is a trade-off between the structural response and the control force, both of which need to be minimized in the control problem. Therefore, the weighting functions W_z and W_u need to be determined considering the performance limit of the structure and the capacity of the control system. As the relative magnitudes of W_g and W_s decide the relative effects of the ground acceleration input and the sensor noise on the control output, they should be determined

considering the input ground acceleration and the sensor noise characteristics applicable to the specific model structure.

3.2. Selection of Weighting Functions

Weighting functions are used to adjust the trade-off problem between the efficient use of the control force and the response reduction. The proper selection of the frequency-dependent weighting functions can specify disturbance attenuation over a desired frequency range, as well as roll off the control action at high frequencies where measurement noise and uncertainties may deteriorate the control performance. In this paper the prototypes of weighting functions and filters are established first, and controllers are designed combining the prototypes. The final controller to be used in the experiment is selected by comparing the performance of the designed controllers. The following are the prototype weighting functions, which are chosen from the shaking-table experiment of the model building with an AMD.

- (i) The earthquake input model W_g represents the frequency spectrum of the earthquake load acting on the structure, and is modeled in such a way that the low-frequency contents are dominant. In this paper, the following two prototypes are used:

$$W_{g1} = \frac{18.7s + 556.8}{s^2 + 12.2s + 364.8} \quad (22)$$

$$W_{g2} = 2.23 \left(\frac{1}{\frac{1}{20}s + 1} \right). \quad (23)$$

Equation (22) is obtained from a Kanai–Tajimi spectrum (Yang et al., 1996) multiplied by a scaling constant. Equation (23) is from the first-order low-pass filter multiplied by a constant 2.23 to make the RMS value for the output have constant value. The low-pass filter enables the input spectrum to decrease in the vicinity of 20 rad s⁻¹. The magnitude of the earthquake input is determined by the constant k_g shown in Figure 5. The constant used k_g in the design of the controller is determined to be 0.04 based on the RMS value of the first 15 s of the 1/3 scaled El Centro earthquake ground acceleration (N–S component).

- (ii) The sensor noise is generally modeled as white noise with constant amplitude in all frequency regions. However, its effect on the measured values tends to be relatively low in the low-frequency region where the responses are large, and tends to be relatively high in the high-frequency region. Considering this, the weighting function for sensor noise is determined as follows:

$$W_{s1} = 0.30 \left(\frac{\frac{1}{60}s + 1}{\frac{1}{200}s + 1} \right) \quad (24)$$

$$W_{s2} = \frac{0.8s^2 + 57.3s + 2991.5}{s^2 + 150.8s + 15791.4}. \quad (25)$$

Equation (24) is obtained by multiplying the high-pass filter by 0.3, and equation (25) is selected to make the magnitude of the second-order transfer function change rapidly.

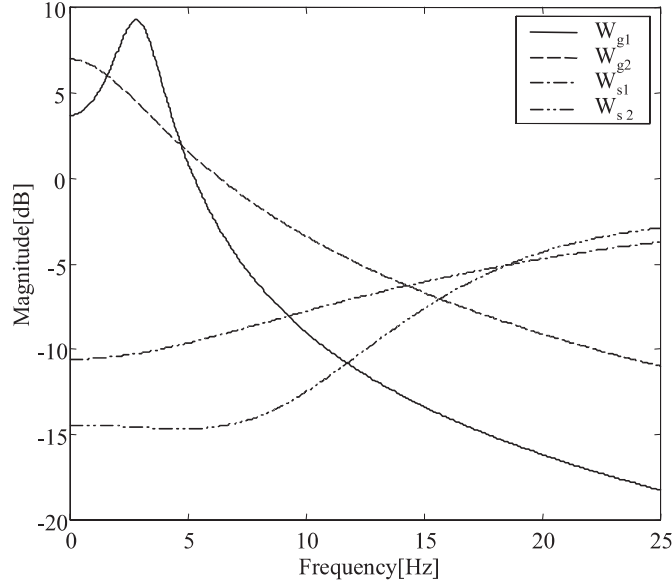


Figure 7. Variation of weighting functions for the earthquake input model (W_g) and sensor noise (W_s).

The coefficient k_s in Figure 5, which determines the magnitude of the sensor noise, is set to be 0.002 based on the RMS value of the sensor noise directly measured from the experiment. The earthquake input model, W_g , and the weighting function for the sensor noise, W_s , provide relatively large weights in low- and high-frequency regions, respectively, which are plotted in Figure 7.

- (iii) As the response of the structure is mostly contributed from the low-frequency components of natural frequencies, it would be necessary to focus the control energy on the low-frequency region. The weighting function for the control output is determined as follows, considering the first and second natural frequencies of the model structure:

$$W_{z1} = 1.5 \quad (26)$$

$$W_{z2} = 1.5 \frac{\frac{1}{300}s + 1}{\frac{1}{30}s + 1} \quad (27)$$

$$W_{z3} = 1.5 \frac{\frac{1}{300}s + 1}{\frac{1}{60}s + 1}. \quad (28)$$

Equations (27) and (28) lead to a decrease in the control energy in the second mode, less than that in the first mode.

- (iv) The higher modes are generally excluded in the process of system identification because their contribution to structural response is not significant. Also, they are difficult to identify. The controller designed in this way, however, cannot secure the controllability of the modes excluded from the system modeling. Therefore, to prevent the spillover

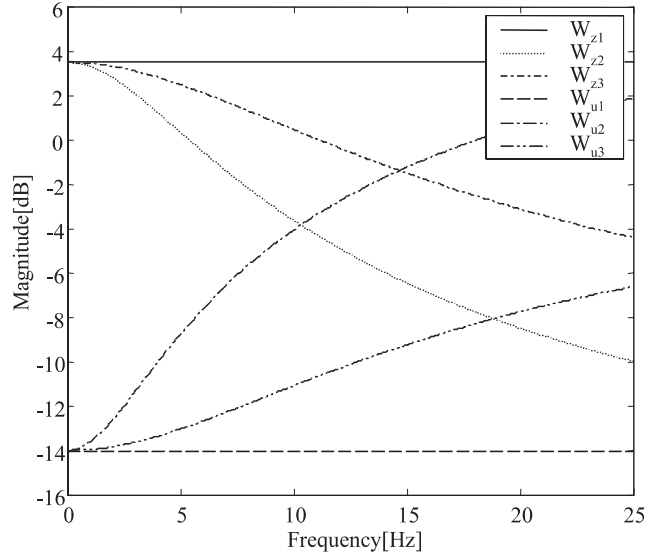


Figure 8. Variation of weighting functions for the absolute acceleration in the third story (W_z) and the control force (W_u).

effect caused by the excitation of the excluded modes, it is necessary to suppress the application of the control force on these modes. Considering this, the following three weighting functions are proposed for the control force:

$$W_{u1} = 0.2 \quad (29)$$

$$W_{u2} = 0.2 \left(\frac{\frac{1}{20}s + 1}{\frac{1}{200}s + 1} \right) \quad (30)$$

$$W_{u3} = 0.2 \left(\frac{\frac{1}{60}s + 1}{\frac{1}{240}s + 1} \right). \quad (31)$$

Equations (29)–(31) decrease the control force in the higher frequencies. The trade-off relation between the weighting functions for control output and control force is mediated by adjusting the relative weights in different frequency regions. The variation of these weighting functions as a function of frequency is plotted in Figure 8.

3.3. Design of Controllers

Different combinations of the various weighting functions described above result in different controllers, and the most efficient one can be selected by comparing the performances of each controller. Table 1 shows the designed controllers with the weights for control output and control force fixed to 1.0 and 0.2, respectively and those for the seismic input and sensor noise varied. To compare the performance of the controllers, the order of the controllers and

Table 1. Design of H_2 controllers using different weighting functions for earthquake input and sensor noise.

Controller	K_1	K_2	K_3	K_4
W_g	1	1	$\frac{18.7s+556.8}{s^2+12.2s+364.8}$	$\frac{18.7s+556.8}{s^2+12.2s+364.8}$
W_s	1	$0.30 \frac{s^{\frac{1}{60}} + 1}{s^{\frac{1}{200}} + 1}$	1	$0.30 \frac{s^{\frac{1}{60}} + 1}{s^{\frac{1}{200}} + 1}$
W_z	1	1	1	1
W_u	0.2	0.2	0.2	0.2
Order	8	11	10	13
$\ H_{z_a w_g}\ _2$	6.8699	6.8613	7.5324	7.8753
$\ H_{z_a w_{s3}}\ _2$	1.4896	1.3965	2.5758	2.4007
$\ H_{u w_g}\ _2$	32.8442	32.8846	40.5519	40.4853
Controller	K_5	K_6	K_7	K_8
W_g	$\frac{18.7s+556.8}{s^2+12.2s+364.8}$	$2.23 \frac{1}{s^{\frac{1}{20}} + 1}$	$2.23 \frac{1}{s^{\frac{1}{20}} + 1}$	$2.23 \frac{1}{s^{\frac{1}{20}} + 1}$
W_s	$\frac{0.8s^2+57.3s+2991.5}{s^2+150.8s+15791.4}$	1	$0.30 \frac{s^{\frac{1}{60}} + 1}{s^{\frac{1}{200}} + 1}$	$\frac{0.8s^2+57.3s+2991.5}{s^2+150.8s+15791.4}$
W_z	1	1	1	1
W_u	0.2	0.2	0.2	0.2
Order	16	9	12	15
$\ H_{z_a w_g}\ _2$	7.8265	6.7594	6.7742	6.7668
$\ H_{z_a w_{s3}}\ _2$	2.5873	1.6456	1.5075	1.5329
$\ H_{u w_g}\ _2$	40.4631	33.7852	33.7982	33.7964

the 2-norms of the transfer functions of the closed-loop system, which excludes weighting functions, are computed and compared. The transfer functions are $H_{z_a w_g}$, $H_{z_a w_{s3}}$, and $H_{u w_g}$, which are the transfer functions from the ground acceleration input to the absolute acceleration at the top floor, from the noise of the top floor sensor to the absolute acceleration at the top floor, and from the ground acceleration input to the control input, respectively. From the results it can be confirmed that there exists a trade-off between control input and reduction of response. Also, it can be observed that the order of controllers depends on the use of the weighting functions. In particular, the weighting function for the sensor noise increases the order of controllers by the order of the weighting function multiplied by the number of sensors, and therefore it would be desirable to implement a low order of weighting functions or no weighting functions at all.

Figures 9 and 10 illustrate the transfer functions of the closed-loop system including the controllers. It can be observed in the figures that the transfer functions increase in the

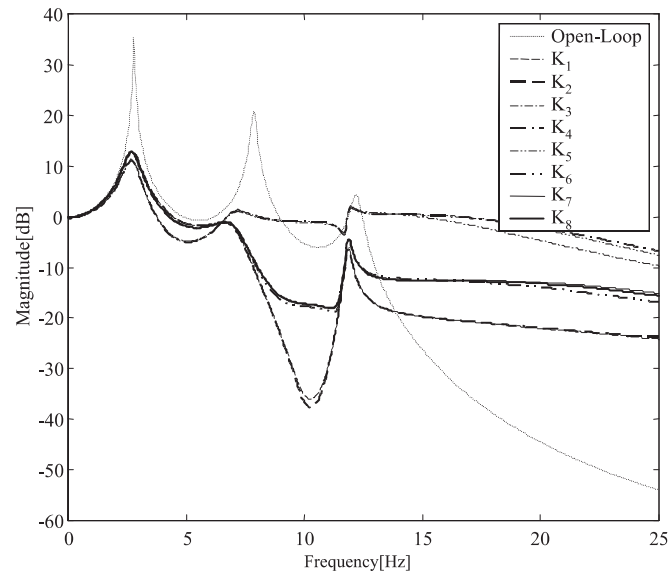


Figure 9. Variation of transfer functions from the ground acceleration input to the acceleration response in the third story.

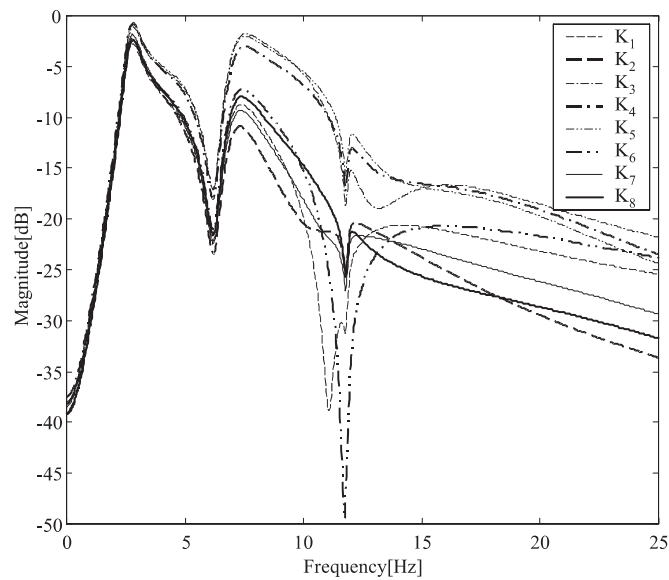


Figure 10. Variation of transfer functions from the sensor noise to the acceleration response in the third story.

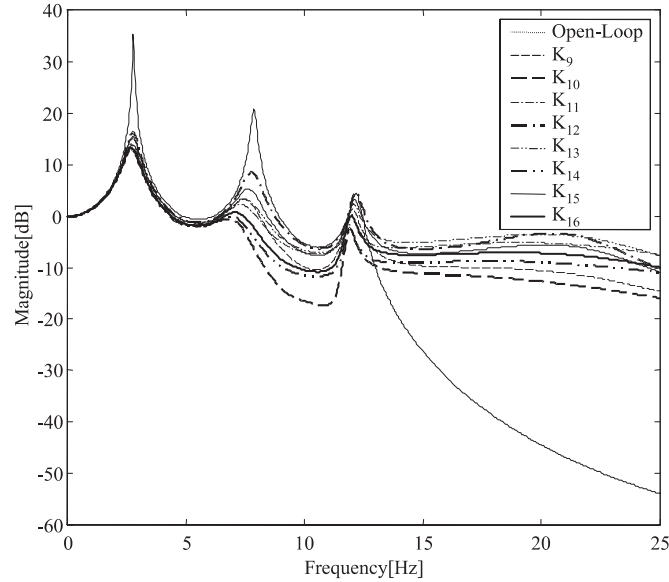


Figure 11. Variation of transfer functions from the ground acceleration input to the acceleration response in the third story.

high-frequency region due to the dynamics of the AMD included in the closed-loop system. The controller \mathbf{K}_6 reduces the responses significantly with small control force and does not increase its transfer function much in the high-frequency region compared to other controllers. Therefore, in this paper the weighting function for the controller \mathbf{K}_6 is selected for the earthquake excitation and sensor noise.

Table 2 shows the results of the controller design, in which the weighting functions W_g and W_s are set to those of the controller \mathbf{K}_6 , and the weighting functions W_z and W_u are varied. Figures 11 and 12 show the variation of two transfer functions as a function of frequency. Comparing the 2-norms of the transfer functions, the controller dimensions, and the transfer functions for each controller case, the controller \mathbf{K}_{10} results in the smallest 2-norm of the transfer function from the ground acceleration input to the third floor acceleration and does not increase the transfer function in the high-frequency region. Therefore, the controller \mathbf{K}_{10} is selected as the final controller to be used in the experiment based on these results.

All the weighting functions and gain parameters, presented above, are derived specifically for the three-story experimental model presented in this paper. Although they are not applicable directly for other structures, the following steps will help the designer implement the proposed procedure in other structures. The first step is to choose the specific control strategy for the target structure. In this paper we adopt the H_2 control strategy, one of the frequency domain optimal control strategies. It has been shown that the H_2 control strategy allows us to specify disturbance attenuation over a desired frequency range, as well as to roll-off the control action at high frequencies where measurement noise and uncertainty may

Table 2. Design of H_2 controllers using weighting functions for control output.

Controller	K_9	K_{10}	K_{11}	K_{12}
W_g	$2.23 \frac{1}{s^{\frac{1}{20}} + 1}$			
W_s	1	1	1	1
W_z	1	1	$\frac{s^{\frac{1}{300}} + 1}{s^{\frac{1}{30}} + 1}$	$\frac{s^{\frac{1}{300}} + 1}{s^{\frac{1}{30}} + 1}$
W_u	$0.2 \frac{s^{\frac{1}{20}} + 1}{s^{\frac{1}{200}} + 1}$	$0.2 \frac{s^{\frac{1}{60}} + 1}{s^{\frac{1}{240}} + 1}$	0.2	$0.2 \frac{s^{\frac{1}{20}} + 1}{s^{\frac{1}{200}} + 1}$
Order	10	10	10	11
$\ H_{z_a w_g}\ _2$	8.3873	7.0240	8.0714	9.8457
$\ H_{z_a w_{s3}}\ _2$	1.4572	1.6069	3.4487	1.8202
$\ H_{u w_g}\ _2$	27.4770	32.6118	30.3372	24.9616
Controller	K_{13}	K_{14}	K_{15}	K_{16}
W_g	$2.23 \frac{1}{s^{\frac{1}{20}} + 1}$			
W_s	1	1	1	1
W_z	$\frac{s^{\frac{1}{300}} + 1}{s^{\frac{1}{30}} + 1}$	$\frac{s^{\frac{1}{300}} + 1}{s^{\frac{1}{60}} + 1}$	$\frac{s^{\frac{1}{300}} + 1}{s^{\frac{1}{60}} + 1}$	$\frac{s^{\frac{1}{300}} + 1}{s^{\frac{1}{60}} + 1}$
W_u	$0.2 \frac{s^{\frac{1}{60}} + 1}{s^{\frac{1}{240}} + 1}$	0.2	$0.2 \frac{s^{\frac{1}{20}} + 1}{s^{\frac{1}{200}} + 1}$	$0.2 \frac{s^{\frac{1}{60}} + 1}{s^{\frac{1}{240}} + 1}$
Order	11	10	11	11
$\ H_{z_a w_g}\ _2$	8.4524	7.1870	8.9455	7.5236
$\ H_{z_a w_{s3}}\ _2$	2.6282	2.4863	1.6592	2.0599
$\ H_{u w_g}\ _2$	29.4431	32.6638	26.7315	31.6122

plague the controlled structure. Once the frequency domain optimal control strategy is chosen, the next step is to select the controller type (the AMD is selected in this paper). Then, based on the system identification experiments of the structure and specific controller type, the frequency-dependent weighting functions are chosen, including filters for the earthquake input model, sensor noise, control output, and control force. The ground acceleration and sensor measurement noise are modeled as white-noise disturbances for the seismic response control system. A low-frequency pass filter is needed for the shaping of the frequency contents of the ground acceleration, such as an earthquake. The Kanai–Tajimi spectrum and the first-order low-pass filter were selected in this paper. Also, a filter is necessary for the sensor noise, which is generally modeled by white noise with constant amplitude in all frequency

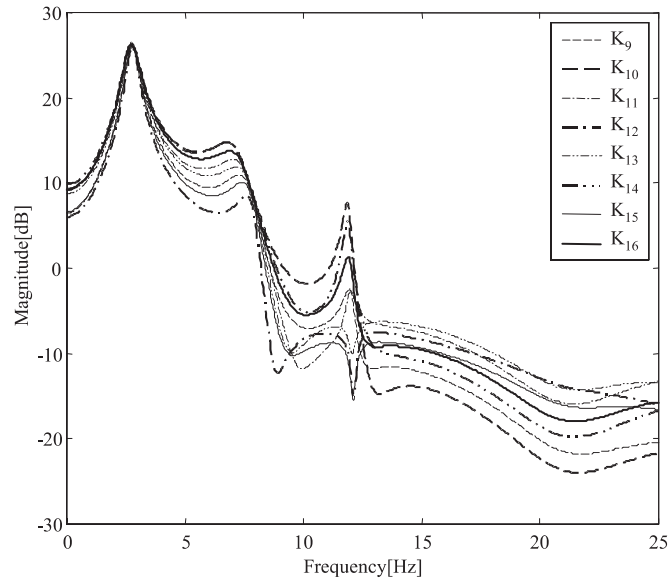


Figure 12. Variation of transfer functions from the ground acceleration input to the control input.

regions. Once the filters are selected, the coefficients should be obtained, which determine the magnitudes of each filter. These were obtained based on the RMS value in this paper. The third step is to determine the weighting function for the control output. As the response of a structure is contributed mostly from the low-frequency components of vibrational modes, the function has a form of low-pass filter including the fundamental natural frequency. The final step is to choose the weighting function to prevent the spillover effect caused by the excitation of the excluded modes. The trade-off between the weighting functions for control output and control force is investigated by adjusting the relative weights of the selected weighting functions. Finally, they are incorporated into the plant to produce an optimal controller by comparing the performance of each controller.

4. EXPERIMENTAL VERIFICATION

To verify the performance of the H_2 controller, which is designed with the selected weight functions (controller \mathbf{K}_{10}), a shaking-table experiment is conducted. The RMS responses for band-limited white noise (10 Hz) and the maximum responses for scaled earthquake records were obtained. For earthquake ground excitations, the velocity records of the following five earthquakes were used: Imperial Valley Earthquake, El Centro (NS); San Fernando Earthquake, Pacoima Dam (S16E); Northridge Earthquake 1, Arleta and Nordhoff Fire Station (NS); Kern Country Earthquake, Taft Lincoln Tunnel (N21E); Northridge Earthquake 2, Santa Monica City Hall Grounds (EW).

Table 3 presents the RMS and the maximum responses in each story obtained from both experiment and numerical simulation. For numerical simulation the ground acceleration

Table 3. Comparison of performance of H_2 controller obtained from experiments and numerical simulations. $f_c(\text{N})$ is control force in Newton.

Response	Simulation		Experiment	
	Uncontrolled	Controlled	Uncontrolled	Controlled
RMS responses of the system for band-limited white-noise (10 Hz) input				
$y_{1st}(\text{g})$	0.0295(100)	0.0133(45.1)	0.0298(100)	0.0121(40.5)
$y_{2nd}(\text{g})$	0.0445(100)	0.0167(37.5)	0.0444(100)	0.0162(36.5)
$y_{3rd}(\text{g})$	0.0574(100)	0.0184(32.0)	0.0571(100)	0.0191(33.6)
$u(\text{V})$	—	0.0956	—	0.0927
$\ddot{x}_d(\text{g})$	—	0.0701	—	0.0547
$f_c(\text{N})$	—	3.3310	—	2.6793
Maximum responses for El Centro earthquake input				
$y_{1st}(\text{g})$	0.0943(100)	0.0774(82.1)	0.0972(100)	0.0639(65.7)
$y_{2nd}(\text{g})$	0.1395(100)	0.0834(59.8)	0.1428(100)	0.0941(65.9)
$y_{3rd}(\text{g})$	0.1679(100)	0.0956(56.9)	0.1778(100)	0.0994(55.9)
$u(\text{V})$	—	0.5130	—	0.5138
$\ddot{x}_d(\text{g})$	—	0.3463	—	0.3813
$f_c(\text{N})$	—	17.5001	—	15.4474
Maximum responses for San Fernando earthquake input				
$y_{1st}(\text{g})$	0.0775(100)	0.0581(74.9)	0.0847(100)	0.0600(70.9)
$y_{2nd}(\text{g})$	0.0989(100)	0.0743(75.1)	0.1034(100)	0.0849(82.1)
$y_{3rd}(\text{g})$	0.1228(100)	0.0707(57.6)	0.1355(100)	0.0845(62.4)
$u(\text{V})$	—	0.3726	—	0.3977
$\ddot{x}_d(\text{g})$	—	0.2310	—	0.2435
$f_c(\text{N})$	—	12.9054	—	10.9222
Maximum responses for Northridge 1 earthquake input				
$y_{1st}(\text{g})$	0.0557(100)	0.0338(60.7)	0.0713(100)	0.0428(60.0)
$y_{2nd}(\text{g})$	0.0872(100)	0.0379(43.4)	0.1056(100)	0.0490(46.4)
$y_{3rd}(\text{g})$	0.1112(100)	0.0399(35.9)	0.1306(100)	0.0541(41.4)
$u(\text{V})$	—	0.2145	—	0.2404
$\ddot{x}_d(\text{g})$	—	0.1510	—	0.1816
$f_c(\text{N})$	—	6.8558	—	7.6083
Maximum responses for Kern County earthquake input				
$y_{1st}(\text{g})$	0.1766(100)	0.0684(38.7)	0.1862(100)	0.0755(40.5)
$y_{2nd}(\text{g})$	0.3061(100)	0.0860(28.1)	0.3140(100)	0.1207(38.4)
$y_{3rd}(\text{g})$	0.4295(100)	0.0959(22.3)	0.4318(100)	0.1156(26.8)
$u(\text{V})$	—	0.4680	—	0.4761
$\ddot{x}_d(\text{g})$	—	0.2951	—	0.3310
$f_c(\text{N})$	—	16.1265	—	14.4510

Table 3. Comparison of performance of H_2 controller obtained from experiments and numerical simulations. $f_c(\text{N})$ is control force in Newton.

Response	Simulation		Experiment	
	Uncontrolled	Controlled	Uncontrolled	Controlled
Maximum responses for Northridge 2 earthquake input				
$y_{1st}(\text{g})$	0.0832(100)	0.0376(45.2)	0.0922(100)	0.0414(44.9)
$y_{2nd}(\text{g})$	0.1242(100)	0.0481(38.7)	0.1324(100)	0.0505(38.1)
$y_{3rd}(\text{g})$	0.1651(100)	0.0506(30.6)	0.1717(100)	0.0610(35.5)
$u(\text{V})$	—	0.2660	—	0.2881
$\ddot{x}_d(\text{g})$	—	0.1762	—	0.1792
$f_c(\text{N})$	—	8.9848	—	7.6088

records measured on the shaking table were used. From the results it can be observed that the responses decrease significantly by applying the H_2 controller. It can also be observed that the results from the numerical analyses coincide well with those from experiments. The terms in parentheses denote the ratio of the controlled response divided by the uncontrolled response. In addition to the comparison of the responses, the command signal to the AMD motor, u , the relative acceleration of the AMD, \ddot{x}_d , and the control force, f_d , are presented. f_d is computed by multiplying the absolute acceleration of the AMD by its moving mass.

Figure 13 shows the response time histories for the El Centro earthquake obtained from shaking-table tests. Considering the limitations imposed on the experimental facilities, the peak ground acceleration of the earthquake was reduced from 0.34 to 0.044 g. From the results it can be noticed that the control efficiency is very low at the beginning of the excitation. This is due to the fact that the controller is designed primarily for the steady state, and is not effective until the transient state is over.

Figure 14 compares the acceleration response in each story obtained from experiments and numerical analyses, where it can be seen that the two results match well considering the existence of noise.

5. CONCLUSIONS

In this paper we have investigated a systematic procedure for determining frequency-dependent weighting functions and filters in designing a frequency domain H_2 controller. Based on the system identification experiments of the model structure and AMD, the frequency-dependent weighting functions were chosen, including filters on earthquake input model, sensor noise, control output, and control force. These were incorporated into the plant to produce an optimal controller. Combining the weighting functions and filters and comparing the trade-off problem between response reduction and control force, an optimal combination of weighting functions and filters was selected. The performance of the designed H_2 controller was validated by a shaking-table test of a scaled model of a three-story shear-building with an AMD.

According to the results from experiments and numerical simulation, the H_2 controller designed in accordance with the proposed procedure turned out to be very efficient at reducing earthquake-induced structural responses.

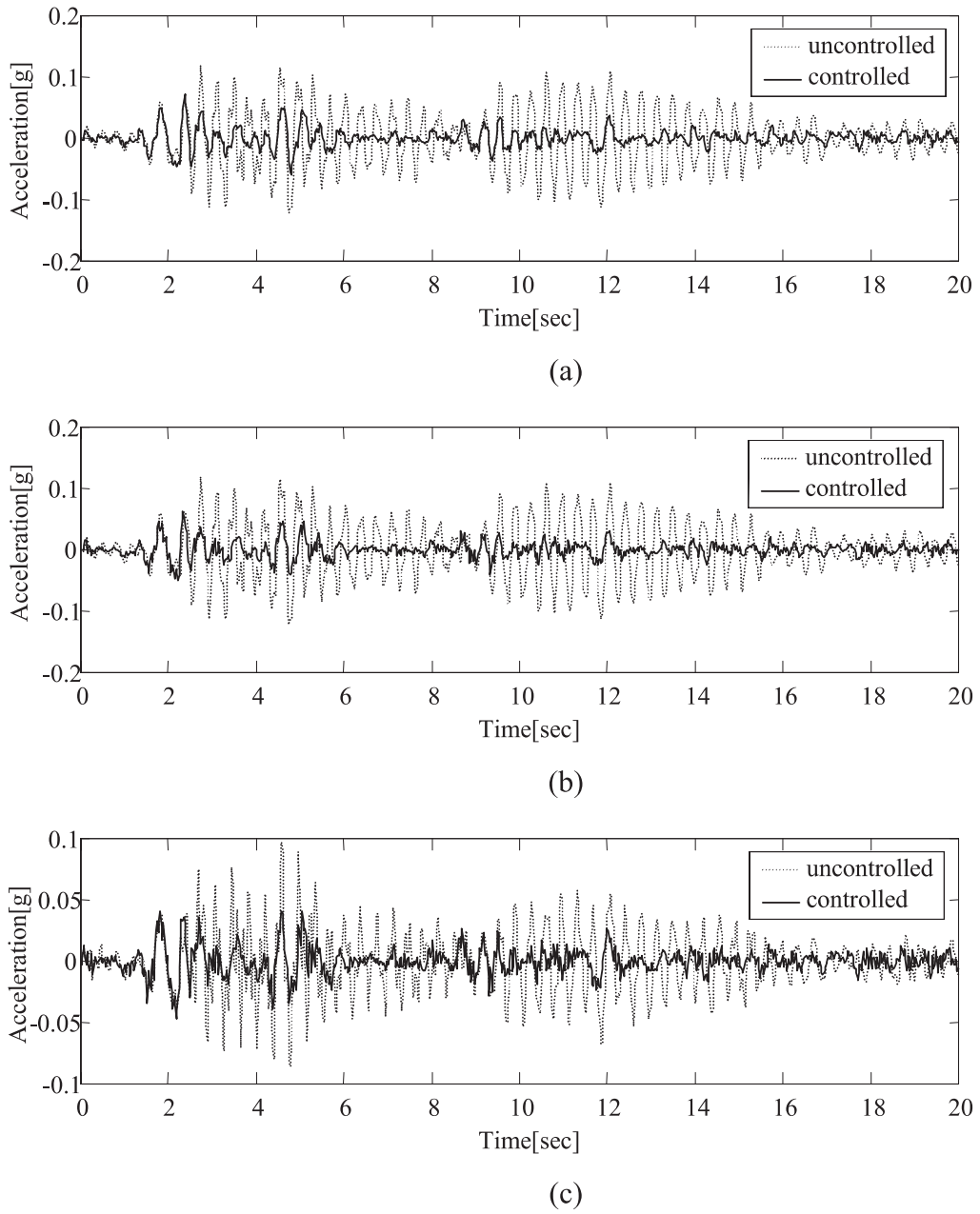
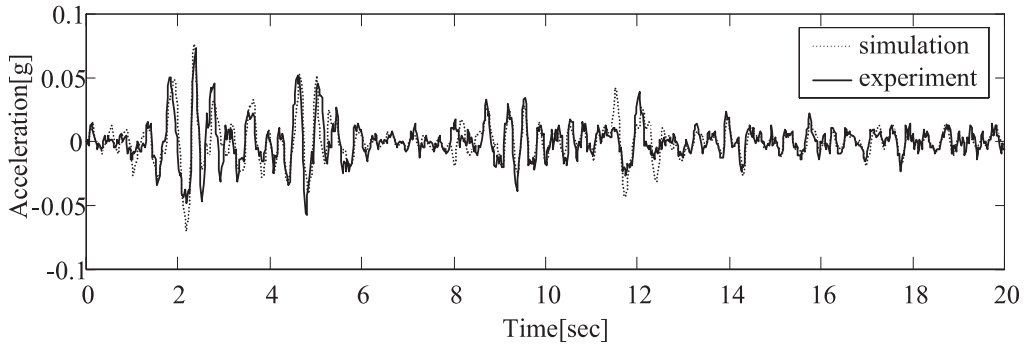
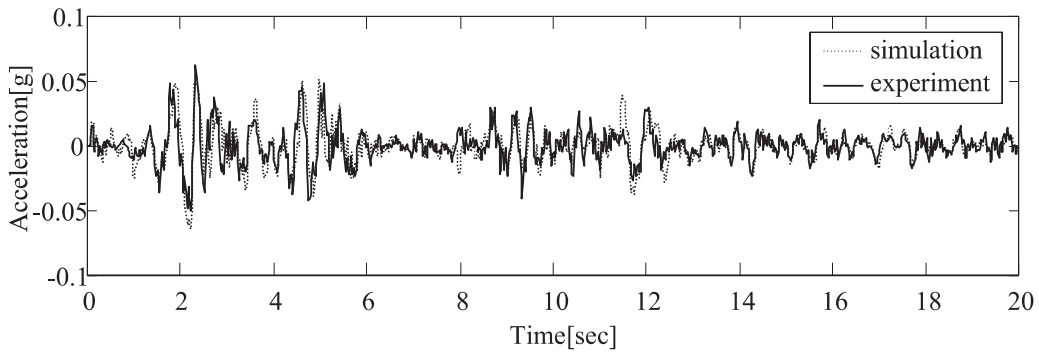


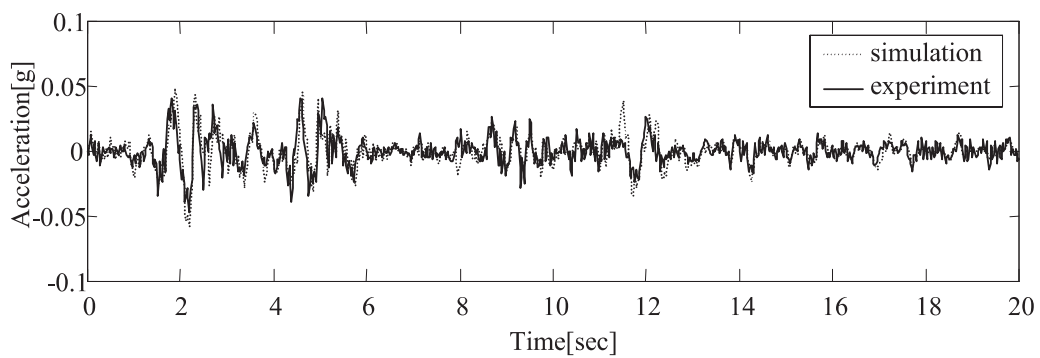
Figure 13. Absolute acceleration responses for El Centro ground excitation (a) in the third story, (b) in the second story, and (c) in the first story.



(a)



(b)



(c)

Figure 14. Comparison of results from the experiment and numerical simulation for El Centro earthquake: acceleration response (a) in the third story, (b) in the second story, and (c) in the first story.

Acknowledgments. The work presented in this paper was supported by the National Research Laboratory Program (Project No. M1-0203-00-0068) from the Ministry of Science and Technology in Korea and the Korea Science and Engineering Foundation (KOSEF) through the Smart Infra-Structure Technology Center (SISTeC) at the Korea Advanced Institute of Science and Technology (KAIST).

REFERENCES

- Boyd, S. P. and Barratt, C. H., 1991, *Linear Controller Design – Limits of Performance*, Prentice-Hall, Englewood Cliffs, NJ.
- Calise, A. J. and Sweriduk, G. D., 1998, “Active attenuation of building structural response using robust control,” *Journal of Engineering Mechanics* **124** (5), 520–528
- Doyle, J. C., Glover, K., Khargonekar, P. P., and Francis, B. A., 1989, “State-space solutions to standard H_2 and H_∞ control problems,” *IEEE Transactions on Automatic Control* **34** (8), 831–847
- Dyke, S. J., Spencer, B. F., Quast, P., Sain, M. K., Kaspari, D. C. Jr, and Soong, T. T., 1994, “Experimental verification of acceleration feedback control strategies for an active tendon system,” Technical Report NCEER-94-0024.
- Housner, G. W. et al., 1997, “Structural control: past, present, and future,” *Journal of Engineering Mechanics* **123** (9), 897–971.
- Spencer, B. F., Suhardjo, J., and Sain, M. K., 1994, “Frequency domain optimal control strategies for aseismic protection,” *Journal of Engineering Mechanics* **120** (1), 135–159.
- Suhardjo, J., Spencer, B. F. Jr, and Kareem, A., 1992, “Frequency domain optimal control of wind-excited buildings,” *Journal of Engineering Mechanics* **118** (12), 2463–2481.
- Yang, J. N., Wu, J. C., Reinhorn, A. M., Riley, M., Schmitendorf, W. E., and Jabbari, F., 1996, “Experimental verification of H_∞ and sliding mode control for seismically excited buildings,” *Journal of Structural Engineering* **122** (1), 69–75.